JOURNAL OF SOLID STATE CHEMISTRY 54, 136–155 (1984)

Localized Moments in the Superconducting $Li_{1+x}Ti_{2-x}O_4$ Spinel System

M. R. HARRISON,* P. P. EDWARDS,*,† AND J. B. GOODENOUGH

Inorganic Chemistry Laboratory, Oxford University, South Parks Road, Oxford OX1 3QR, United Kingdom

Received November 7, 1983; in revised form March 19, 1984

Electron spin resonance (ESR) and magnetic-susceptibility measurements on the $Li_{1+x}Ti_{2-x}O_4$ spinel system ($0 \leq x \leq \frac{1}{3}$) indicate the presence of two types of localized moments in this material. In both cases, an unpaired electron is trapped as a Ti^{3+} ion in a crystal field that is predominantly octahedral, but with a strong tetragonal component. This type of crystal field cannot arise in the stoichiometric spinel. We propose two types of defect in the title spinel system: an oxygen vacancy and a hydroxyl ion. Unpaired electrons are trapped as Ti^{3+} ions adjacent to these defects, and it is argued that the strong tetragonal field is associated with the formation of a static $(TiO)^+$ ion by a displacement of the titanium ion from the defect. Spin relaxation occurs via a thermal ionization of the trapped electron that appears to be associated with a static–dynamic transition in the titanium-ion displacement.

Introduction

The spinel system $Li_{1+x}Ti_{2-x}O_4$ ($0 \leq x \leq \frac{1}{3}$) has attracted considerable attention following the discovery by Johnston *et al.* (*1*) of superconducting transition temperatures $T_c \simeq 11$ K in the compositional range $0 \leq x \leq 0.1$. The disappearance of superconductivity above $x = 0.1$ prompted Johnston *et al.* (*2–5*) to suggest it was due to a metal–insulator transition (MIT) at that composition, but the nature of the MIT was not resolved. Other groups have attempted to improve the superconducting properties of the spinel phase (*6–10*), but none has addressed seriously the MIT. We have studied this spinel system in detail (*11*), and in a further paper we report our investigations of the MIT (*12*).

A puzzling feature of the magnetic-susceptibility (*3*) and heat-capacity (*4*) measurements was the presence of localized moments in both metallic and insulating compositions at a concentration much higher than expected from foreign-atom magnetic impurities. In order to identify the origin of these moments, we chose to study the low-temperature electron spin resonance (ESR) spectra and magnetic susceptibility of various compositions within the homogeneity range $0 \leq x \leq \frac{1}{3}$. We report here our results, which reveal localized Ti^{3+} ions only in octahedral sites that are strongly perturbed by defects in the structure. We were unable to detect any resonance from the Ti^{3+} ions in the remaining octahedral sites, and this is attributed to an extremely rapid spin relaxation of these

* Present address: University Chemical Laboratory, Cambridge University, Lensfield Road, Cambridge CB2 1EW, UK.

† To whom correspondence should be addressed.

0022-4596/84 $3.00

Ti^{3+} ions in both metallic and insulating compositions.

At temperatures above 30 K, an axially symmetric resonance was observed over almost the entire compositional range, $0 \leq x \leq \frac{1}{3}$. From the theory of Ti^{3+}-ion g-values, we show that this resonance is due to a Ti^{3+} ion in an octahedral crystal field having a strong tetragonal component. We assign this to an octahedral-site Ti^{3+} ion adjacent to an oxygen vacancy.

Below 30 K, a more complex spectrum was observed from samples with high values of x, $0.2 \leq x \leq \frac{1}{3}$; it consisted of a superposition of a second resonance on the axially symmetric resonance found above 30 K. A similar spectrum was observed from samples of $Li_{4/3}Ti_{5/3}O_4$ ($x = \frac{1}{3}$) that had been reduced in hydrogen at elevated temperatures. The second resonance is shown to be from a Ti^{3+} ion in an octahedral field with a different strong tetragonal component. We assign this to an octahedral-site Ti^{3+} ion adjacent to a hydroxyl ion, with the opposite oxide ion coordinated by two octahedral-site lithium ions.

The $Li_{1+x}Ti_{2-x}O_4$ Spinel System

The spinel structure (Fig. 1) consists of a cubic close-packed array of anions with cations occupying, in an ordered manner, one-eighth of the tetrahedral (A) sites and one-half of the octahedral (B) sites. In a normal spinel all the A cations are similar, and all the B cations are similar. The positions of the A and B cations are fixed by the symmetry of the structure, but the positions of the anions can vary and are specified by the value of a single anion parameter, u. If the origin of the unit cell is fixed at the center of symmetry of the structure, a value of $u = 0.25$ corresponds to perfect close-packing of the anions. Generally the anions are displaced from these ideal positions in a ⟨111⟩ direction away from the A cations; for a normal spinel this displacement is toward the center of an equilateral triangle of B cations. This movement ($u > 0.25$) enlarges the tetrahedral sites without distorting the tetrahedral symmetry of the crystal field; it compresses the octahedral sites and reduces the trigonal component of the octahedral-site crystal field that is established by the cation order.

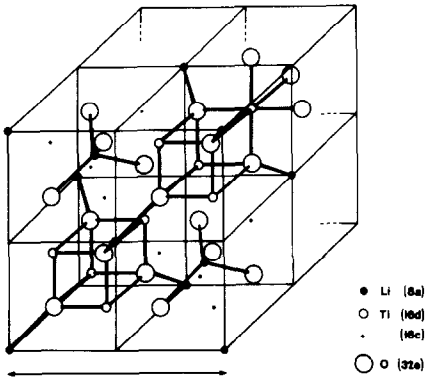

FIG. 1. The spinel structure of $LiTi_2O_4$ showing the A-sites (8a), B-sites (16d) and unoccupied interstitial sites (16c). The site labels are taken from Ref. (*46*). For clarity, the origin of the unit cell is taken as an A-site in this figure. An alternative origin at the center of symmetry of the structure is common and is used in the text. The two origins are related by a translation of $(\frac{1}{8}, \frac{1}{8}, \frac{1}{8})$ (*46*).

In the $Li_{1+x}Ti_{2-x}O_4$ system, the covalency of the titanium-3*d* orbitals and the higher charge of the titanium ions gives the titanium ions a strong preference for the octahedral sites relative to the lithium ions. Using X-ray diffraction methods, Johnston (*3*) deduced that the A sites in the $Li_{1+x}Ti_{2-x}O_4$ system are indeed occupied entirely by lithium ions and that the B sites are *randomly* occupied by x lithium ions and $(2 - x)$ titanium ions per formula unit.

Figure 2 shows the anticipated band structure for a metallic composition. Each titanium ion resides at the center of a trigonally distorted octahedron, and the titanium-3*d* orbitals are split by the cubic component of the crystal field into more stable $^2T_{2g}$ and less stable E_g orbitals. The $^2T_{2g}$ orbitals are then further split by the trigonal

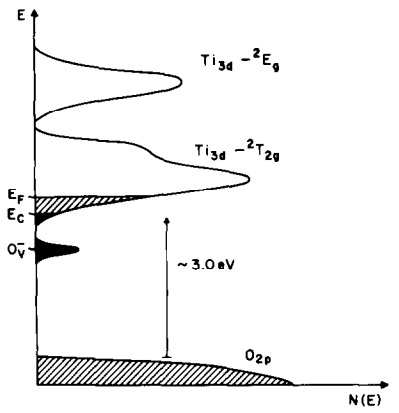

FIG. 2. The band structure of a metallic sample of $Li_{1+x}Ti_{2-x}O_4$ with an intermediate value of x. Lightly shaded states in the Ti_{3d} bands are occupied by itinerant electrons; heavily shaded states by localized electrons. States labeled O_V^- arise from electrons trapped at oxygen vacancies (see text for details).

component of the crystal field. The octahedra share edges with each other, and the titanium–titanium separation through the edges of the octahedra decreases from 2.972 Å for $LiTi_2O_4$ ($x = 0$) to 2.955 Å for $Li_{4/3}Ti_{5/3}O_4$ ($x = \frac{1}{3}$) (*11*). Cation–cation interactions therefore play a dominant role in the formation of a titanium-3*d* conduction band from the $^2T_{2g}$ orbitals that is one-twelfth full in metallic $LiTi_2O_4$ ($x = 0$) and empty in $Li_{4/3}Ti_{5/3}O_4$ ($x = \frac{1}{3}$) (*13*). Diffuse-reflectance measurements show that the bottom of the titanium-3*d* conduction band lies approximately 3 eV above the oxygen-2*p* valence band (*11*).

As the Fermi energy, E_F, moves down towards the bottom of the conduction band with increasing x, it is of interest to know how the transition from metallic to insulating behavior takes place. Substitution of B-site titanium ions by lithium ions changes the electronic properties of the material in two ways: it perturbs the conduction band and it reduces the concentration of titanium-3*d* electrons in the conduction band. A random distribution of lithium ions will result in the introduction of a mobility edge, E_c, separating localized ($E_c > E$) and itinerant ($E > E_c$) electron states (*14*) (Fig. 2). As x increases, the mobility edge increases in energy and the Fermi level, E_F, decreases in energy. According to the Anderson model, the MIT would then occur at the composition where E_c is equal to E_F (*14*). The results obtained by Johnston *et al.* (*2–5*) on the $Li_{1+x}Ti_{2-x}O_4$ system were indeed consistent with the occurrence of an Anderson MIT at $x = 0.1$, since an activation energy appeared in the electrical conductivity of the nonmetallic state without any abrupt change in the density of states at the Fermi level. However, the nature of the MIT is rather more complex than this simple model, and is discussed more fully in a forthcoming paper (*12*).

Experimental Methods

Samples were prepared as polycrystalline powders by heating together mixtures of lithium titanate and titanium oxides (Ventron Alfa). Following Deschanvres *et al.* (*15*), lithium titanate was used instead of lithium carbonate to minimize the loss of lithium oxide during the firing under vacuum. Loss of lithium oxide would be expected to create oxide-ion vacancies in the samples, and the precise nature of these defects is considered in the Discussion section. Initially, the lithium titanate was prepared from lithium carbonate (BDH):

$$Li_2CO_3 + TiO_2 \rightarrow Li_2TiO_3 + CO_2(g). \quad (1)$$

The constituents were ground, pressed into pellets, and then fired at 800°C in oxygen for 8 hr in an alumina boat lined with gold foil. X-ray analysis of the product showed only the monoclinic phase of Li_2TiO_3 (*16*) but this phase has a large homogeneity range (*3*) and so it would be possible for the product to be deficient in lithium oxide. To minimize this possibility, the majority of the samples were prepared using lithium titanate of known stoichiometry (Ventron Alfa). In fact, no difference was detected in the properties of the spinel samples pre-

pared using these different batches of lithium titanate. The spinel phase was prepared:

$$(1 + x)Li_2TiO_3 + (1 - 3x)Ti_2O_3 + (1 + 3x)TiO_2 \rightarrow 2Li_{1+x}Ti_{2-x}O_4. \quad (2)$$

The constituents were again ground and pressed into pellets. With the exception of $Li_{4/3}Ti_{5/3}O_4$, which was fired in oxygen, the pellets were fired at 800°C under vacuum for 16 hr in an alumina boat lined with gold foil. In addition, each of the pellets was individually wrapped in gold foil to further minimize the loss of lithium oxide during the firing. This temperature was found to be optimum; below ~700°C the starting materials failed to react, and above ~900°C the ramsdellite phase formed instead of the spinel phase (*17–21*). The vacuum was maintained at better than 10^{-3} Torr throughout the firing. Finally, the samples were ground to a fine powder and stored in an evacuated dessicator; no visible deterioration of the samples was observed under these conditions over a period of several months. Examination of the powders under an electron microscope indicated a uniform particle size of ~5 μm.

X-Ray diffraction data were obtained with a Philips diffractometer equipped with a diffracted-beam crystal monochromator, using Cu$K\alpha$ radiation. The oxygen parameter, u, was refined from the integrated peak intensities (*22*). This involved a least-square refinement[1] of the intensities of nine diffraction lines and three parameters: a scale factor, the oxygen parameter, and an isotropic temperature factor.

ESR spectra of the powdered samples sealed in Spectrosil silica tubes were recorded on a Varian E-109 spectrometer at X-band frequencies (9.3 GHz) using a 100-kHz modulation frequency. The temperature of the samples could be continually varied between 15 and 120 K using helium gas, and between 120 K and room temperature using nitrogen gas. The temperature was measured with a thermocouple positioned in the gas flow path just below the samples, and could be controlled to within 2 K by means of an Air Products regulator. The g-values were calculated to within 0.002 using a substitution method with DPPH as a standard ($g = 2.0036$).

The onset of superconductivity in the samples was studied using a mutual-inductance apparatus operating at a frequency of 400 Hz. The detection system of this apparatus consisted of a primary coil with two opposed secondary coils wound symmetrically about it. The sample was placed in one of the secondary coils, and the onset of superconductivity was indicated by an imbalance between the secondary coils due to the abrupt increase in the magnetic shielding that occurred when the sample became diamagnetic. The temperature was measured with a calibrated Cryo-Cal germanium sensor, which had been checked against the known transition temperature of niobium. The T_c value was taken as the temperature at which the inductively-measured transition was half-complete; the width of the transition was defined as the temperature difference between the points where the transition was 10 and 90% complete. To obtain a quantitative indication of the fraction of the samples undergoing a transition to the superconducting state, the magnetic susceptibility of the samples was measured below T_c in a very small magnetic field using a SQUID magnetometer. The details of these measurements are described in the Results section.

The magnetic susceptibility of the samples was also measured from 4 K (or T_c) to room temperature using a high-sensitivity Faraday balance. The samples were held in Spectrosil silica buckets suspended from a Cahn electrobalance by a silica rod. The

[1] Thanks are due to Dr. P. J. Wiseman, Dept. of Inorganic Chemistry, Oxford University, for the use of his computer program.

temperature was controlled to within 0.2 K by means of a Janis Dewar flask containing a silicon diode sensor, and a microprocessor was used to automate the data acquisition. The balance was calibrated using $HgCo(SCN)_4$ as a standard. All samples were run over a range of fields (5–10 kG); susceptibilities were found to be field-independent. The reported susceptibilities have been corrected for the susceptibility of the silica buckets, and the estimated accuracy of the measurements is $\sim 2 \times 10^{-6}$ cm^3 mole^{-1}.

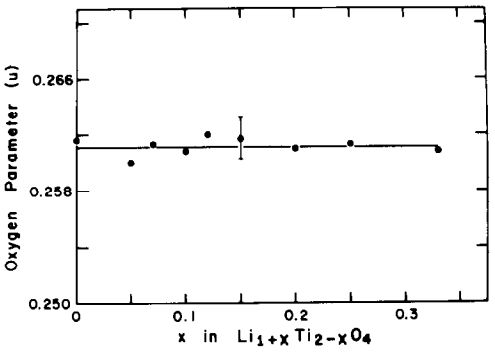

FIG. 4. Oxygen parameter, u, as a function of x in $Li_{1+x}Ti_{2-x}O_4$.

Results

X-Ray Measurements

X-Ray analysis of the product generally showed only the spinel phase of $Li_{1+x}Ti_{2-x}O_4$. However, samples with values of x near to 0.1 showed some weak lines belonging to an unknown impurity phase; investigations showed that this impurity phase was concentrated near the surface of the fired pellet and could be mostly removed by surface grinding.

Figure 3 shows the variation of the cubic lattice parameter, a, with the nominal composition, x, of the samples; it is linear, with a least-square fit giving

$$a = (8.407 - 0.143x)\ \text{Å}, \qquad (3)$$

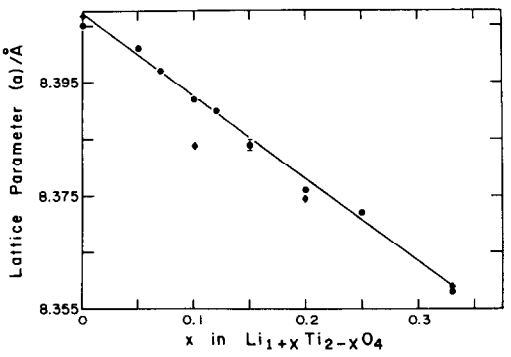

FIG. 3. Lattice parameter, a as a function of x in $Li_{1+x}Ti_{2-x}O_4$. Values obtained by Johnston (*3*) are shown by the diamond symbols.

and a correlation coefficient of 0.997. Also shown are the values obtained by Johnston (*3*); he reports very similar values for the end members of the system, but lower values for samples with values of x near to 0.1. This discrepancy may be caused by a partial oxidation of Johnston's samples due to their preparation in sealed silica tubes (*11*), and we discuss the differences in the preparation procedures in another paper (*12*). If this is indeed the reason for the discrepancy, the titanium-3d electron concentration in Johnston's $x = 0.1$ sample is reduced to the electron concentration expected for a sample with $x \sim 0.15$ (see below).

Figure 4 shows that the refined oxygen parameter, u, is effectively constant over the entire homogeneity range of the system, with a mean value of 0.261 ± 0.001 (if the origin of the unit cell is fixed at the center of symmetry of the structure).

General Features of the ESR Spectra

ESR spectra at 25 K for several samples with compositions spanning the homogeneity range from $x = 0$ to $x = 0.25$ are shown in Fig. 5. No ESR signal was observed from unreduced samples of $Li_{4/3}Ti_{5/3}O_4$ ($x = \frac{1}{3}$). It was difficult to tune the microwave cavity due to the high electrical conductivity of the samples with low values of x. Roy *et al.* (*7*) showed that the electrical conductivity

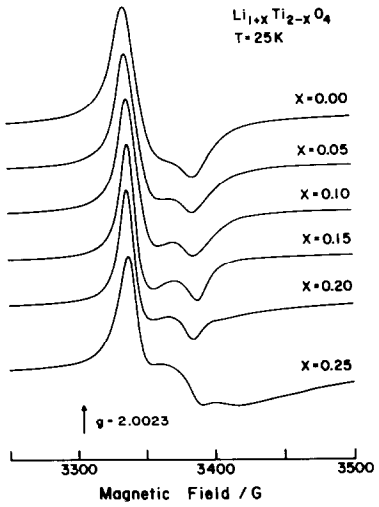

FIG. 5. ESR spectra (9.3 GHz—25 K) of samples of $LI_{1+x}Ti_{2-x}O_4$.

of $LiTi_2O_4$ ($x = 0$), the most conducting of the compositions, was approximately 5000 Ω^{-1} cm^{-1}; so the skin depth for microwave penetration is calculated to be ~5 μm at a frequency of 9.3 GHz. This penetration depth is therefore comparable with the grain size of the powder. That the microwaves penetrate to a considerable extent into the bulk of the samples is confirmed by the Lorentzian lineshape exhibited by the resonances (see below); a Dysonian lineshape occurs if the skin depth is much smaller than the particle dimensions (*23*).

The spectra for samples with $x = 0$, $x = 0.05$, $x = 0.1$, and $x = 0.15$ are characteristic of those of an axially symmetric species, while the spectra for samples with $x = 0.2$ and $x = 0.25$ are more complex. However, the variation of the spectra with composition is continuous, and there is no evidence of any discontinuities in either the g-values, linewidth, or lineshape over the entire series. Our discussion of the ESR spectra is divided into three parts: vacuum-fired samples with low values of x; vacuum-fired samples with high values of x (with an arbitrary-dividing line taken at $x = 0.2$); and samples of $Li_{4/3}Ti_{5/3}O_4$ ($x = \frac{1}{3}$) reduced in hydrogen at elevated temperatures.

$0 < x < 0.2$. A comparison of observed and simulated spectra for vacuum-fired samples with $x = 0$ and $x = 0.15$ is shown in Fig. 6. The dots define the simulated spectra (*24*) and the solid lines are the observed spectra. The isotropic linewidths of the simulated spectra were $\Delta B_{1/2} = 13.5$ G for the $x = 0$ spectrum, and $\Delta B_{1/2} = 9.5$ G for the $x = 0.15$ spectrum ($\Delta B_{1/2}$ is defined as the full-width at half-height of the absorption curve). A Lorentzian lineshape was used in the simulation. At 25 K the fit is very good for both the $x = 0$ and $x = 0.15$ spectra, indicating that the resonances do indeed have axial symmetry and a Lorentzian lineshape. In this composition range, the g-values giving the best (visual) fit to the observed spectra are ($g_y = g_x$):

$$g_x = 1.979 \pm 0.002$$
$$g_z = 1.951 \pm 0.002. \qquad (4)$$

In the remainder of this paper, we shall refer to this ESR signal as resonance I.

Below 120 K, the linewidth of the resonance increases slowly with temperature.

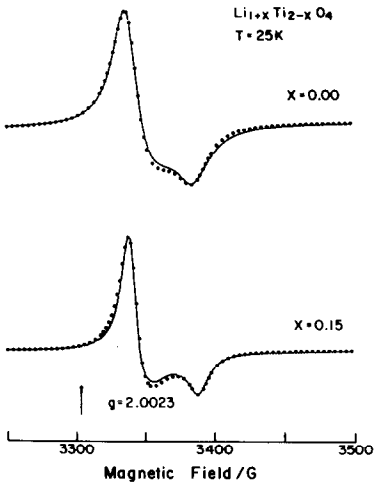

FIG. 6. ESR spectra (9.3 GHz—25 K) of $LiTi_2O_4$ ($x = 0$) and $Li_{1.15}Ti_{1.85}O_4$ ($x = 0.15$), together with the dotted simulated spectra (see text for details).

Above 120 K, the linewidth increases much more rapidly with temperature, as shown in Fig. 7 (ΔB_{pp} is measured between the low-field and high-field peaks of the derivative spectrum). This spin-lattice relaxation could occur via a Raman (*25*) or resonant-Raman process (*26*); the integrated intensity of the absorption spectrum should then decrease with temperature according to a Curie–Weiss law. Alternatively, spin-lattice relaxation could occur via thermal ionization of the localized moment out of the trap state into the titanium-3*d* conduction band (*27*). This would cause a similar line broadening and simultaneously decrease the integrated intensity of the absorption spectrum at a rate faster than predicted by the Curie–Weiss law. Moreover, the linewidth at a given temperature would be a sensitive indicator of the depth of the trap state. At present, we cannot unambiguously distinguish between these possibilities, but in the Discussion section we argue in favor of a thermal ionization mechanism for resonance I.

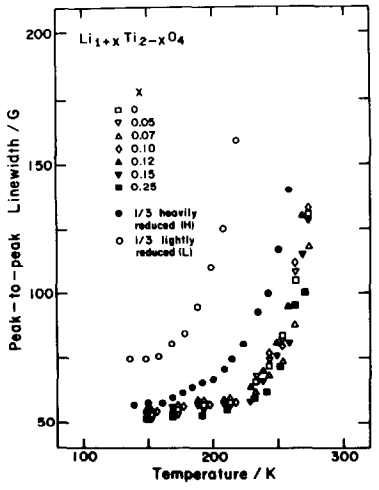

FIG. 7. Peak-to-peak linewidth (ΔB_{pp}) of the derivative ESR spectrum as a function of temperature for vacuum-fired samples of $Li_{1+x}Ti_{2-x}O_4$ ($x < \frac{1}{3}$) and samples of $Li_{4/3}Ti_{5/3}O_4$ ($x = \frac{1}{3}$) lightly (L) and heavily (H) reduced in hydrogen.

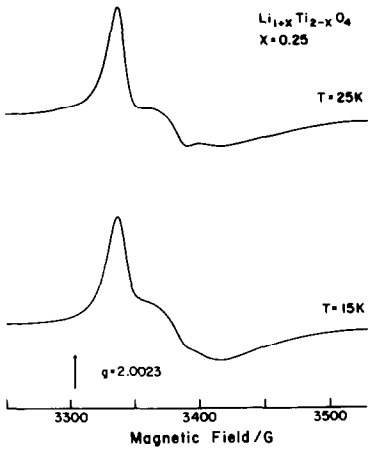

FIG. 8. ESR spectra (9.3 GHz—25 and 15 K) of $Li_{1.25}Ti_{1.75}O_4$ ($x = 0.25$).

$0.2 < x < \frac{1}{3}$. Vacuum-fired samples in this compositional range exhibit considerably more complex ESR spectra (Fig. 5). In particular, a characteristic feature in the ESR spectra at 25 K is the presence of an absorption tail extending far into the high-field region of the spectra. Computer-simulation studies point to the presence of two overlapping signals: a contribution from the resonance I identified in the samples with low values of x and a contribution from a second resonance. The latter signal also has approximate axial symmetry, but it is not possible to accurately determine the g-values from these spectra. We shall refer to this signal as resonance II.

In Fig. 8 we show the spectrum obtained from the sample with $x = 0.25$ at a lower temperature, 15 K, together with the corresponding spectrum at 25 K. It is apparent that the intensity of resonance II decreases very rapidly with increasing temperature. This temperature-dependent behavior could originate in any of the ways described previously, viz. Raman, resonant-Raman, or thermal ionization. However, our observations on hydrogen-reduced samples in which the same resonance II is observed at a much higher temperature (see below)

again support thermal ionization as being the most realistic mechanism. Further support of this assignment comes from the compositional dependence of the intensity of resonance II; where Ti^{3+} ions are present ($x < \frac{1}{3}$) the intensity is greatest in the composition with the greatest lithium fraction, and it decreases as the concentration of lithium ions decreases. The significance of this dependence is considered in the Discussion section.

Hydrogen-Reduced Samples of $Li_{4/3}Ti_{5/3}O_4$ ($x = \frac{1}{3}$)

In order to compare the defects observed in the spinel system with the well-documented situation for reduced samples of TiO_2 (*11, 28–30*), several samples of $Li_{4/3}Ti_{5/3}O_4$ ($x = \frac{1}{3}$) were reduced in hydrogen at different temperatures and for different periods of time. No ESR signal was observed from these materials prior to reduction. The original white powder turns blue, with the depth of the color depending upon the degree of reduction. Figure 9 shows the ESR spectrum of a lightly reduced sample, hereafter labeled L. The experimental conditions were reduction at 750°C for 4 hr in pure hydrogen. The g-values estimated from the turning points in the first-derivative spectrum were ($g_y \simeq g_x$)

$$g_x = 1.984 \pm 0.002$$

$$g_z = 1.946 \pm 0.002. \quad (5)$$

Comparing Figs. 8 and 9, it appears that once resonance I is subtracted from the resonance of the sample with $x = 0.25$, the two ESR spectra exhibit similar features. In particular the absorption tail extending into the high-field region of the spectrum is prominent in both cases. Therefore, we identify resonance II with a defect created by light reduction, which we assume to be the hydroxyl ion (see below). However, in contrast to the resonance II observed in the sample with $x = 0.25$ where the ESR signal had essentially vanished at 30 K, the resonance II observed in the sample L remained visible to at least 200 K (Fig. 7).

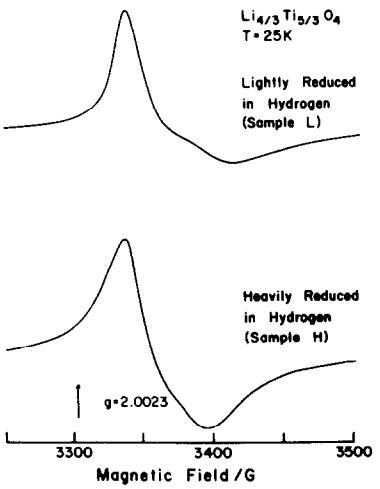

FIG. 9. ESR spectra (9.3 GHz—25 K) of $Li_{4/3}Ti_{5/3}O_4$ ($x = \frac{1}{3}$) lightly (L) and heavily (H) reduced in hydrogen.

Figure 9 also shows the ESR spectrum of a heavily reduced sample, hereafter labeled H. The experimental conditions were 850°C for several periods of 4 hr in pure hydrogen. The absorption tail at the high-field side of the spectrum is much less pronounced in sample H than in sample L, and the peaks defining the g-values of the spectrum have moved closer together. The resonance is also more intense than the resonance from sample L. It would appear that this resonance contains a strong contribution from resonance I as well as a contribution from resonance II.

Magnetic Susceptibility Measurements

Samples in the compositional range $0 \leq x \leq 0.15$ were found to be superconducting above 4.2 K, and their superconducting properties are summarized in Table I. As the lithium fraction in the samples increases, the T_c values remain approximately constant at ~11 K in the composition range $0 \leq x \leq 0.1$ and then decrease slowly for higher values of x. They are simi-

TABLE I

SUPERCONDUCTING PROPERTIES OF $Li_{1-x}Ti_{2-x}O_4$

Composition x	Transition temperature[a] (K)	Transition width[a] (K)	Signal strength[b]
0.00	11.0	3.0	100
0.05	10.5	3.2	61
0.07	10.4	3.2	42
0.10	10.3	3.9	28
0.12	9.4	3.0	17
0.15	[c]	[c]	2

[a] Measured using a mutual-inductance magnetometer.

[b] Measured using a SQUID magnetometer at 4.2 K. Values are relative to $LiTi_2O_4$ ($x = 0$).

[c] Signal strength too low for a transition to be detected.

lar to the values obtained from heat-capacity measurements by Johnston *et al.* (*4*) for equivalent compositions except for the case of $x = 0.1$ where they obtained $T_c = 9.6$ K. However, correcting the nominal composition of this sample to an "effective" composition of $x \sim 0.15$ as discussed above produces better agreement of the T_c values. In contrast to the small variation in the T_c values, the relative strength of the superconducting transitions decrease rapidly over the composition range $0 \leq x \leq 0.15$. Before considering these results, it is necessary to indicate how the fraction of the samples undergoing a superconducting transition was determined.

The volume magnetic susceptibility of a bulk superconductor has the value $(-\frac{1}{4})\pi$, and so a measurement of the diamagnetic susceptibility should enable the superconducting fraction of the sample to be determined. The diamagnetic susceptibility of a nonbulk superconductor, however, is sensitive to the disposition of the superconducting fraction within the nonsuperconducting material. For example, an enhanced diamagnetic susceptibility may be observed if the superconducting fraction is localized on the surface of the material. Heat-capacity measurements provide a more reliable indication of the superconducting fraction, and Johnston *et al.* (*4*) demonstrated that $LiTi_2O_4$ ($x = 0$) is indeed a bulk superconductor. In the present investigation the diamagnetic susceptibility of all the superconducting samples was then measured at 4.2 K in a very small magnetic field ($\sim 0.00005T$) to obtain an indication of the fraction of each sample that was superconducting relative to the sample of $LiTi_2O_4$. These measurements are approximate for the reason given above but they do demonstrate that the superconducting fraction decreases rapidly as the lithium fraction increases, with only a very small fraction of the $x = 0.15$ sample becoming superconducting.

The occurrence of weak superconductivity in compositions above the MIT at $x = 0.1$ suggests the presence of chemical inhomogeneities in the samples. Isolated regions of the B-cation sublattice that are deficient in lithium ions may support superconductivity even if the bulk of the sample does not. Such chemical inhomogeneities suggest an instability to disproportionation, and in another paper we discuss this point in more detail (*12*). Because of these inhomogeneities, however, the transition will be "smeared out" over a range of compositions centered at $x = 0.1$.

Figure 10 shows the variation of the molar magnetic susceptibility, χ, with temperature for three compositions with $x = 0$, $x = 0.15$, and $x = 0.25$. The ESR measurements support Johnston's hypothesis (*3*) that the magnetic susceptibility may be analyzed as the sum of two components: a contribution from localized electrons trapped as Ti^{3+} ions; and a weakly temperature-dependent contribution from the conduction electrons. Above T_c, the measured molar magnetic susceptibility may therefore be separated into a Curie–Weiss term, $C_m/(T + \theta)$, and a weakly temperature-dependent term, $f(T)$:

$$\chi = C_m/(T + \theta) + f(T). \qquad (6)$$

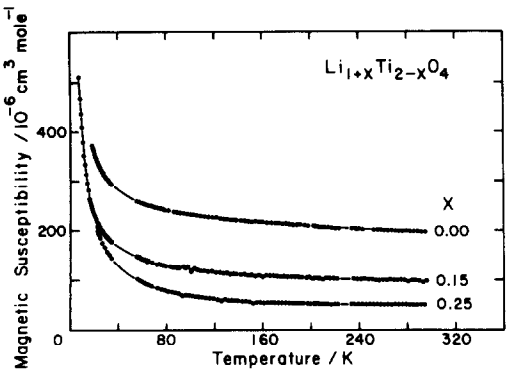

FIG. 10. Molar magnetic susceptibility, χ, as a function of temperature for three samples of $Li_{1+x}Ti_{2-x}O_4$. The data has been fitted to the equation $\chi = C_m/(T + \theta) + f(T)$, where $f(T) = A_m + B_mT$.

Experiment showed that $f(T)$ may be suitably parameterized in the form:

$$f(T) = A_m + B_mT. \quad (7)$$

Figure 10 provides evidence of the excellent fit of the data to Eq. (6); the solid curves through the data points represent the fitted functions. The fitted parameters of the Curie–Weiss term are given in Table II, which shows that the Curie constants are similar to the values obtained by Johnston (*3*) for equivalent compositions. These parameters describe the magnetic susceptibility of the localized moments, and Table II also shows the concentration of localized moments in the samples assuming that all of the moments have spin one-half ($g \sim 2$). If it is further assumed that all of the moments arise from electrons trapped as Ti^{3+} ions, we can calculate the percentage of titanium-3*d* electrons that are localized, and the percentage of titanium sites that are occupied by these localized titanium-3*d* electrons. There is no systematic variation of these quantities with the lithium fraction of the samples, suggesting that any variation in the concentration of the localized moments arises from slight variations in the preparation conditions of the samples. Experiment showed that the concentration of localized moments increases if the samples are fired at higher temperatures, or for a longer time. It is not possible to significantly reduce the concentration of localized moments by reducing the firing temperature or time, how-

TABLE II

MAGNETIC MOMENTS IN $Li_{1+x}Ti_{2-x}O_4$

Composition x	Curie constant C_m (10^{-6} cm^3 mole^{-1})	Weiss constant θ (K)	Concentration of localized moments (10^{20} cm^{-3})	Percentage of titanium-3*d* electrons that are localized	Percentage of titanium sites with electrons that are localized
0.00	2780	−0.9	1.01	0.75	0.37
	(1300)	[a]	(0.47)	(0.35)	(0.17)
0.05	7050	0.1	2.56	2.23	0.97
0.07	7570	0.5	2.75	2.58	1.06
0.10	3770	1.6	1.37	1.45	0.53
	(6100)	[a]	(2.22)	(2.34)	(0.86)
0.12	3300	2.5	1.20	1.38	0.47
0.15	3170	2.5	1.16	1.55	0.46
0.20	5860	1.0	2.14	3.94	0.88
	(4300)	[a]	(1.57)	(2.89)	(0.64)
0.25	4470	2.1	1.64	4.81	0.69

[a] Set to zero when fitting data above 4 K. Data below 4 K for $Li_{1.2}Ti_{1.8}O_4$ ($x = 0.2$) gave $C_m = 5000 \times 10^{-6}$ cm^3 mole^{-1} and $\theta = 0.8$ K (*3*). Bracketed values from Ref. (*3*).

ever, since the starting materials do not then react to form the spinel phase.

It is likely that the majority of the localized moments observed in the magnetic-susceptibility measurements originate from electrons trapped at defect sites I, and the integrated intensity of the ESR signal from resonance I was found to be compatible with this hypothesis. However, it is probable that more than one species of trapped electron is present in the samples with high values of x. Besides the electrons trapped at defect sites I and II detected by ESR, electrons may be trapped as Ti^{3+} ions on normal B-sites in the insulating compositions. These electrons would not be detected by ESR due to the extremely rapid spin relaxation of the Ti^{3+} ions in these sites.

Jonnston *et al.* (*3, 4*) studied the magnetic susceptibility and heat capacity of a nonsuperconducting $x = 0.2$ sample down to ~1 K. The magnetic susceptibility measurements showed the presence of additional localized moments in this sample at these low temperatures (see the footnote in Table II) and the heat capacity measurements showed the high-temperature tail of a Schottky anomaly. An extremely weak Schottky anomaly was also detectable in the $x = 0.1$ sample ("effective" composition $x \sim 0.15$). Both the additional moments and the Schottky anomaly may arise from the species responsible for resonance II since we are only able to detect this resonance at low temperatures in the samples with $x = 0.2$ and $x = 0.25$. Alternatively, they may arise from a species not detected in the ESR measurements such as electrons trapped as Ti^{3+} ions on normal B-sites in the insulating compositions. Further low-temperature measurements on samples with high values of x would be of interest.

We finally consider the magnetic susceptibility of the conduction electrons, which is obtained by subtracting the contribution of the localized moments from the experimental data. We first have to subtract the temperature-independent contribution of the ion cores. Johnston (*3*) showed that the diamagnetic susceptibility of the ion cores happened to cancel the second-order temperature-independent paramagnetic susceptibility of the titanium ion-cores coordinated by oxygen octahedra; the magnetic susceptibility of the oxidized composition $Li_{4/3}Ti_{5/3}O_4$ ($x = \frac{1}{3}$) was measured to be $\sim 1 \times 10^{-6}$ cm^3 mole^{-1}. This value is very small compared to the values measured in the samples with $x < \frac{1}{3}$ (Fig. 10) and may be neglected. Thus the term $f(T)$ represents the magnetic susceptibility of the conduction electrons.

Figure 11 shows the variation of $f(T)$ with temperature, and demonstrates that $f(T)$ fits extremely well to a linear variation with temperature. The fitted values of A_m and B_m are plotted as a function of nominal composition in Figs. 12 and 13, respectively. Also shown are the magnetic susceptibility values obtained by Johnston (*3*) for equivalent compositions. These points represent the magnetic susceptibility of the samples at 50 K after subtraction of the contribution from the localized moments. There is good agreement for the samples with $x = 0$ and $x = 0.2$, but poorer agreement in the case of the sample with $x = 0.1$. However, correcting the nominal composition of this sample

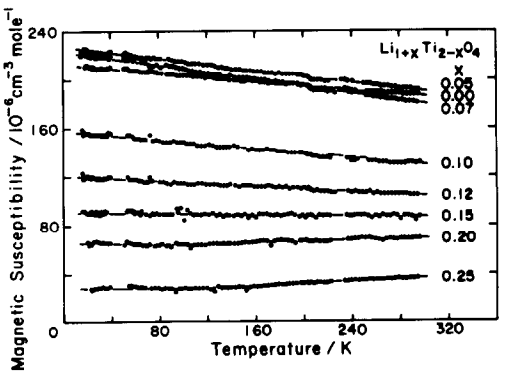

FIG. 11. $f(T) = A_m + B_m T$ as a function of temperature for samples of $Li_{1+x}Ti_{2-x}O_4$.

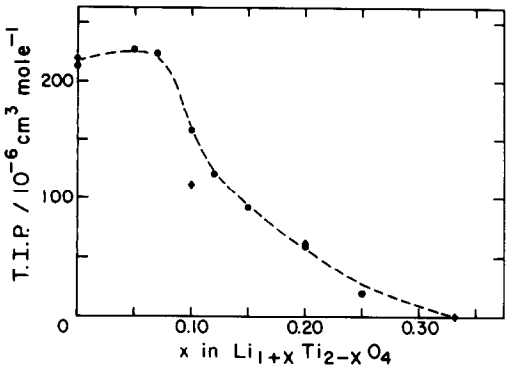

FIG. 12. A_m as a function of x in $Li_{1+x}Ti_{2-x}O_4$. Values obtained by Johnston (*3*) are shown by the diamond symbols.

to an "effective" composition of $x \sim 0.15$ as discussed above produces better agreement. The A_m values remain approximately constant in the composition range $0 \leq x \leq 0.07$ and then decrease for higher values of x above the MIT. Of particular interest is the variation of the B_m values with composition; there is a transition from a negative slope ($B_m < 0$) in the samples with low values of x through to a positive slope ($B_m > 0$) in the samples with high values of x. The largest magnitude of B_m occurs close to the MIT. Further analysis of this data necessitates a discussion of the origin of the term, $f(T)$ and this is considered in another paper (*12*).

Discussion

Reduction Processes

The formation of localized moments at lattice defects can be achieved by a variety of reactions:

(*1*) *Insertion of Hydrogen into the Lattice*

The low-temperature (light) reduction of $Li_{4/3}Ti_{5/3}O_4$ ($x = \frac{1}{3}$) by molecular hydrogen most likely occurs by a dissociation of H_2 into atomic hydrogen on the surface, followed by a diffusion of the atoms into the bulk of the material. It then proceeds via the reaction:

$$O^{2-} + H \rightarrow e^- + [H^+ + O^{2-}]. \quad (8)$$

e^- represents an electron in the titanium-3*d* conduction band, and the complex $[H^+ + O^{2-}]$ represents a proton trapped in the Coulomb field of an oxide ion. This is usually described as a "hydroxyl ion" of overall stoichiometry $(OH)^-$. This hydroxyl ion may then trap a single conduction-band electron on a neighboring titanium ion at low temperatures and give rise to an ESR signal (resonance II). A detailed description of such a defect center is given later in this paper.

Even for the vacuum-fired samples with $x < \frac{1}{3}$, hydrogen may be implicated in the creation of defects. This is certainly true in the case of TiO_2. Although reduction of TiO_2 was generally assumed to occur upon heating under clean vacuum conditions as well as upon heating in hydrogen, it has now been demonstrated that *no* reduction occurs upon heating under UHV conditions for temperatures as high as 1000°C (*31*); the previously observed vacuum reduction of TiO_2 and creation of an ESR signal (*32*) was most likely due to contamination of the vacuum system with hydrogen. In moderate vacuum preparations (ca. 10^{-4} Torr) hydrogen as an impurity will *always* be present to

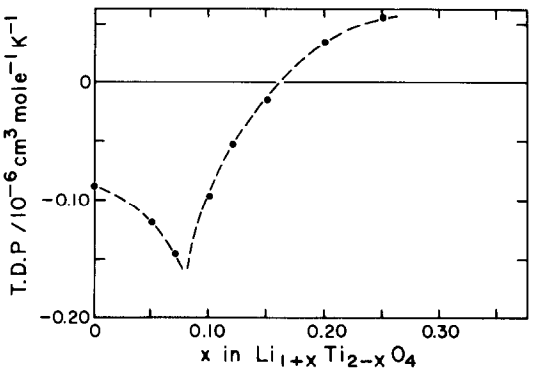

FIG. 13. B_m as a function of x in $Li_{1+x}Ti_{2-x}O_4$.

permit a degree of reduction to occur at fairly low temperatures.

(2) *Removal of Oxygen from the Lattice*

The high-temperature (heavy) reduction most likely proceeds via the removal of oxygen atoms from the sample. There are three probable reactions capable of producing an ESR signal at low temperatures:

(*i*) *Loss of H_2O:*

$$O^{2-} + 2H \rightarrow 2e^- + O_v + H_2O(g). \quad (9)$$

O_v represents an oxide-ion vacancy that may then trap two conduction-band electrons. However, our measurements show that only a single conduction-band electron is trapped on one of the three neighboring titanium ions, giving rise to an ESR signal (resonance I). We refer to this defect center as an O_v^- center, and a detailed description of such a defect center is also given later in this paper. The remaining conduction-band electron is *not* trapped even at the lowest temperatures.

(*ii*) *Loss of Li_2O.*

$$2Li^+ + O^{2-} \rightarrow 2A_v + O_v + Li_2O(g). \quad (10)$$

A_v represents an *A-site* lithium-ion vacancy. The oxide-ion vacancy may then trap one conduction-band electron to form the O_v^- defect center as described above. In this case, however, the conduction-band electron is not created with the defect, but is removed from the existing population of titanium-3*d* electrons determined by the nominal stoichiometry of the material.

(*iii*) *Loss of O_2.*

$$2O^{2-} \rightarrow 4e^- + 2O_v + O_2(g). \quad (11)$$

In this case, the oxygen is removed directly from the lattice. In TiO_2 this reaction does not occur below 1000°C (*31*), so reactions (9) and (10) are much more likely to occur than reaction (11) under the present experimental conditions; viz., exposure to pure hydrogen at 850°C.

These oxygen and A-site lithium-ion vacancies are generated at the surface; they ultimately diffuse into the bulk of the material. It has been proposed that the presence of hydrogen within a material significantly enhances the rate of diffusion of oxygen vacancies from the surface to the interior of the sample (*33*). As indicated above, the hydrogen forms hydroxyl ions, and the lower charge of the hydroxyl ions relative to the oxide ions reduces the activation energy required for an oxide ion (and hence an oxygen vacancy) to move from site to site. A lithium-ion mobility even at room temperature has been demonstrated (*11*).

It is necessary to consider whether, once within the bulk of the material, the oxygen vacancies are eliminated by the formation of shear planes. Shear planes have been clearly demonstrated in reduced TiO_2 (rutile) (*34*), and the concentration of oxygen vacancies in single-crystal samples is very small (much higher concentrations appear to occur in polycrystalline samples due to the much higher surface area in these samples (*11*)). We do not possess single-crystal samples of the title spinel system, and so we cannot directly compare the defect properties of the two systems. However, it has been proposed that shear-plane formation may be correlated with the dielectric properties of a material (*34*). Compounds in which shear planes are formed are generally found to have very high values of the static dielectric constant, whereas compounds in which oxygen vacancies are formed have low values. The static dielectric constant of TiO_2 (rutile) is ~150 (*34*) whereas the static dielectric constant of $Li_{4/3}Ti_{5/3}O_4$ ($x = \frac{1}{3}$) is 11 (*3*). This low value suggests that shear-plane formation in the $Li_{1+x}Ti_{2-x}O_4$ system is unlikely, and that significant concentrations of oxygen vacancies can occur in both polycrystalline and single-crystal samples.

Possible Trap Sites

Experiments with sample H have indi-

cated a strong correlation between resonance I and the preparation conditions capable of forming oxygen vacancies. Similarly, experiments with sample L have indicated a strong correlation between resonance II and the preparation conditions compatible with the introduction of hydrogen and the formation of hydroxyl ions. We now argue that each of these resonances is only compatible with a *strong* tetragonal component superimposed on an octahedral crystal field. We further argue that such a strong tetragonal component of the crystal field requires a displacement of a titanium ion away from the defect to form a $(TiO)^+$ "titanyl" ion with the oxide ion *opposite* the defect. We will then conclude that the associated defects are an oxygen vacancy for resonance I, and a hydroxyl ion for resonance II. However, it is also necessary to consider: (1) why a triangular-cluster molecular orbital composed of titanium-3*d* orbitals from the three titanium ions neighboring the oxygen vacancy is not formed, and (2) why the energy of the doubly occupied oxygen vacancy O_v^{2-} is raised above E_F; i.e., a second conduction-band electron is *not* trapped even at the lowest temperatures.

The ESR signals are characteristic of electrons trapped at Ti^{3+} ions, and titanium ions have a strong preference for the octahedral sites. Therefore we need only consider octahedral-site Ti^{3+} ions in the following discussion. In the space group $Fd3m$ appropriate to the spinel structure, these consist of the B sites (16d) and the interstitial sites (16c) (Fig. 1). An octahedral field splits the ^2D free-ion Ti^{3+} ground state into an orbital-triplet $^2T_{2g}$ state lying some 10^4 cm^{-1} below an orbital-doublet ^2E_g state. The electronic g-values then depend sensitively upon the nature and magnitude of any distortion of the crystal field from pure octahedral symmetry.

In the ideal spinel $LiTi_2O_4$ ($x = 0$), both the B sites and the interstitial sites have a trigonal component to the crystal field that is established by the cation order and by the anion displacements represented by a value of $u > 0.25$. For each of the B-site ions of the unit cell, the trigonal-field axis is along the $\langle 111 \rangle$ direction. This axial component of the crystal field leaves the upper ^2E_g level orbitally twofold-degenerate, but it splits the $^2T_{2g}$ level into a lower orbital-singlet $^2A_{1g}$ state and a higher orbital-doublet ^2E_g state. The magnitude of this trigonal-field splitting is reduced if $u > 0.25$, and the sign of the splitting may even be reversed for large u as shown in Fig. 14(a). Since the trigonal-field splitting is small, the orbital angular momentum associated with the ^2E_g state of $^2T_{2g}$ parentage is not quenched even with the stabilization of the $^2A_{1g}$ state, so the spin–orbit interactions must always be added to give three Kramer's doublets.

We take the trigonal axis as the z axis and neglect mixing with the upper E_g manifold. The calculated g-values for a ^2E_g ground state (large u) are then both close to zero as the orbital and spin contributions cancel (*35*). The calculated g-values for a $^2A_{1g}$ ground state (small u) are (*35*)

$$g_x = \frac{(2\gamma - 3\lambda)}{\sqrt{((\lambda + 2\gamma)^2 + 8\lambda^2)}} + 1$$
$$g_z = \frac{3(2\gamma + \lambda)}{\sqrt{((\lambda + 2\gamma)^2 + 8\lambda^2)}} - 1 \qquad (12)$$

where γ is the trigonal-field splitting (Fig. 14(a)), and λ is the spin–orbit coupling constant (154 cm^{-1} for Ti^{3+} ions (*36*)). The spin–orbit coupling constant may be reduced in a crystal from the free-ion value; this reduction may be taken into account by the introduction of an isotropic "orbital-reduction factor," k, where k is less than one (*37*). The λ in Eq. (12) is then replaced everywhere by $k\lambda$.

It can be shown that the g-values calculated from Eq. (12) obey the inequality $g_z > g_x$ for any magnitude of the distortion (*35*). Thus, for *neither* of the two possible trigonal ground states do we obtain $g_x > g_z$ as

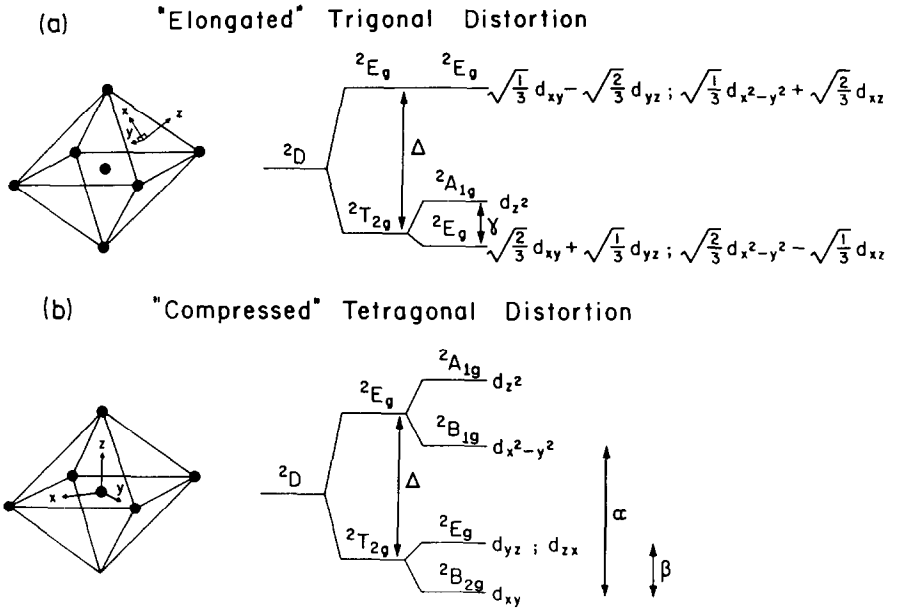

FIG. 14. Energy levels and wavefunctions for (a) an "elongated" trigonal distortion and (b) a "compressed" tetragonal distortion of the octahedral sites.

observed in the ESR spectra. Moreover, it can be shown that a similar result holds even if a mixing of the $^2T_{2g}$ and ^2E_g manifolds is considered (*38, 39*).

From these considerations, it follows that the ESR signals do not arise from Ti^{3+} ions in octahedral sites having a trigonal component to the crystal field; they must come from Ti^{3+} ions in octahedral sites having a small net trigonal-field component that is totally dominated by some other axial field. This other axial field must also be strong enough to dominate any effects from B-site lithium-ion nearest neighbors in samples with $x > 0$.

The alternative axial field to consider is tetragonal, and we now take the tetragonal axis as the z axis. A tetragonal distortion of an octahedral field splits not only the $^2T_{2g}$ orbital-triplet state into an orbital-doublet ^2E_g state and an orbital-singlet $^2B_{2g}$ state, but also splits the upper ^2E_g orbital-doublet state into $^2A_{1g}$ and $^2B_{1g}$ orbital-singlet states (Fig. 14(b)). For a tetragonal distortion, it is important to take this splitting of the states in the ^2E_g manifold into account when calculating the g-values. For an "elongation" along the z axis, the calculated g-values for the ^2E_g ground state are both close to zero as the orbital and spin contributions cancel (*40*). For a "compression" along the z axis, stronger covalent mixing along this axis raises the anti-π-bonding d_{yz} and d_{zx} orbitals relative to the d_{xy} orbital, and the anti-σ-bonding d_{z2} orbital relative to the d_{x2-y2} orbital. The calculated g-values for a $^2B_{2g}$ (d_{xy}) ground state and a *weak* tetragonal distortion still do not generate the inequality $g_x > g_z$ (*40*). However, for a *strong* tetragonal distortion an inequality $g_x > g_z$ is possible. The calculated g-values for a $^2B_{2g}$ (d_{xy}) ground state are (*41*) (see Fig. 14(b) for the definition of α and β):

$$g_x = 2 - (2\lambda/\beta)$$
$$g_z = 2 - (8\lambda/\alpha). \qquad (13)$$

An orbital-reduction factor can similarly be introduced into the spin-orbit coupling parameter as in Eq. (12). It follows from Eq.

(13) that $g_x < g_z$ for $\alpha > 4\beta$ (weak-field), but that $g_x > g_z$ can be attained in a strong enough tetragonal field such that $\alpha < 4\beta$. More elaborate calculations to higher order give a similar result (*41*).

In the Appendix, an angular-overlap model is used to compare calculated g-values for a Ti^{3+} ion in a normal B site and in a site with an oxygen vacancy at one corner. It is apparent that an oxygen vacancy can produce a tetragonal field of sufficient magnitude and of the correct sign to make $g_x > g_z$, as observed in resonance I.

The Oxygen Vacancy Defect

We now consider in more detail the character of the O_v^- center. As illustrated in Fig. 15, an anion vacancy creates an imbalance in the Ti–O bonding that results in a titanium-ion displacement toward the oxide ion on the opposite side. The titanium ions neighboring an oxygen vacancy thus occupy square-pyramidal sites. In the case of Ti^{4+} or Ti^{3+} ions, the apical Ti–O distance may be particularly shortened; spontaneous ferroelectric distortions to form a short Ti–O bond occur, for example, in $BaTiO_3$ (*42*). These displacements produce a tetragonal crystal field equivalent to a "compression," thus giving the correct sign of the axial field. Moreover, occupancy of the d_{xy} orbital does not interfere with the strong

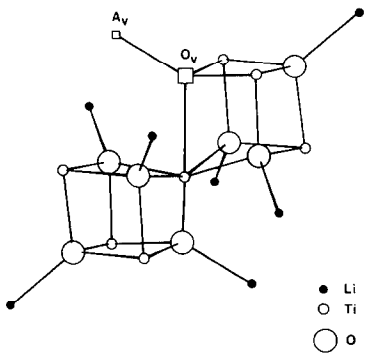

FIG. 15. The oxygen vacancy defect center responsible for resonance I.

π and σ bonding via empty d_{yz}, d_{zx}, and d_{z^2} orbitals, so a short apical Ti–O distance can be maintained on reduction of the titanium from Ti^{4+} to Ti^{3+}, which is analogous to the situation at a vanadyl cation, $(VO)^{2+}$ (*43*). Therefore we refer below to $(TiO)^{2+}$ and $(TiO)^+$ ions to emphasize the short Ti–O bond in the square-pyramidal site.

An isolated oxygen vacancy normally traps two spin-paired localized electrons below the bottom of a conduction band composed of d states. This is nicely illustrated by the MIT in EuO_{1-z} (*44*). In our system, resonance I is associated with the trapping of a single unpaired localized electron down to the lowest temperatures. This presumably means that the O_v^{2-} level lies above the Fermi energy, E_F, in Fig. 2. We need to ask why this might happen.

In the rocksalt structure of EuO_{1-z}, the O_v states are *symmetrized* cation orbitals split off from the conduction band. The octahedral-cluster molecular orbital formed from europium-5*d* orbitals at the six Eu^{2+} ions neighboring an isolated oxygen vacancy in EuO_{1-z} has a relatively large radial extension, so the electron–electron electrostatic energy, U, separating energies of the O_v^- and O_v^{2-} states is relatively small; viz. $U \simeq 0.5$ eV. In the "non-ideal" spinel $Li_{1-y}Ti_2O_{4-z}$ ($x = 0$), an oxygen vacancy has three titanium nearest neighbors, and these could form a triangular-cluster molecular orbital. However, such a molecular orbital would have a strong trigonal-field axis along the ⟨111⟩ direction (Fig. 1) and so cannot give rise to the observed resonance I. Therefore we are forced to conclude that the titanium-ion displacements away from the oxygen vacancy destabilize the π-bonding d_{yz} and d_{zx} orbitals (the z axes at each neighboring titanium ion are taken to be parallel to a displacement direction and hence orthogonal to one another) sufficiently to lift any triangular-cluster molecular orbital above E_F, leaving below E_F the three orthogonal d_{xy} orbitals of the $(TiO)^{2+}$

ions. Trapping an electron at one of these d_{xy} orbitals creates an O_v^- center.

The demands of local charge neutrality would then be expected to stabilize an O_v^{2-} center in which two of the nearest-neighbor $(TiO)^{2+}$ ions trapped electrons in orthogonal d_{xy} orbitals; these electrons would then couple ferromagnetically via a direct exchange to give a triple ($S = 1$) trap state rather than a singlet ($S = 0$) trap state. However, the electrostatic energy dictated by the requirements for local charge neutrality would be offset by a relatively large U associated with localized d_{xy} electrons in neighboring $(TiO)^+$ ions. Since the lithium ions are mobile in this system (*11*), the two A-site lithium-ion vacancies A_v created by reaction (10) along with the oxygen vacancy are also mobile. These vacancies may be attracted to the oxygen vacancy to give, for example, an A_v–O_v^- cluster having a net neutral charge (Fig. 15). This clustering would raise the energies of the O_v^- and O_v^{2-} states sufficiently to raise the energy of the O_v^{2-} state above E_F. Reaction (10) should dominate the mechanism for oxygen-vacancy creation in the vacuum-fired samples and be an important constituent in the heavily reduced sample H. Therefore, we conclude that resonance I is due to an electron trapped on a titanium ion next to an oxygen vacancy with a strong possibility of an associated A-site lithium-ion vacancy.

The Hydroxyl-Ion Defect

Experiment has shown that resonance II is associated with both hydrogen and *B-site* lithium ions. Figure 16 represents a model that tries to take all these factors into account. If a hydroxyl ion replaces an oxygen vacancy, a similar bonding imbalance is introduced as the proton competes for the oxide-ion electrons. Although a static displacement of the titanium ion away from the hydroxyl ion provides a net gain in energy that increases with the displacement, the total energy gain is significantly less

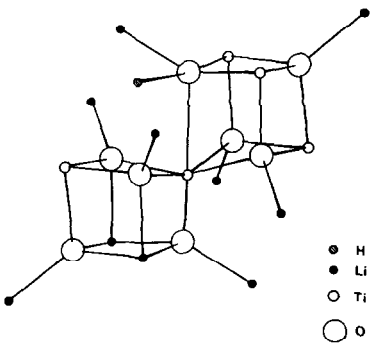

FIG. 16. The hydroxyl-ion defect center responsible for resonance II.

than if a vacancy was there. Therefore the titanium-ion displacement is reduced, and we should anticipate a weaker tetragonal field. However, the g-values of resonance II in sample L would indicate that the defects associated with the insertion of hydrogen have at least as great a tetragonal component of the field as that produced by an oxygen vacancy. Therefore the defect centre associated with the hydroxyl ions must be more complex.

In the end member $Li_{4/3}Ti_{5/3}O_4$ ($x = \frac{1}{3}$), there is a high probability that a given B-site titanium ion has two lithium ions among its six B-site nearest neighbors. If these lithium ions are on adjacent B-sites as shown in Fig. 16, the titanium ion would bond most strongly to the oxide ion that bonds to the three lithium ions. If, in addition, a hydrogen atom forms a hydroxyl ion on the opposite side of the titanium ion, the resulting Ti^{3+} ion will be displaced toward the oxide ion to form a $(TiO)^+$ ion. The asymmetric coordination of positive charge would provide an electrostatic energy that reinforced the stabilization associated with increasing the Ti–O π and σ bonding with the oxide ion coordinated to three lithium ions at the expense of the Ti–O bonding to the hydroxyl ion; it would also tend to twist the axis of the $(TiO)^+$ ion away from the ⟨001⟩ direction, thus skewing the shape of the resonance.

Spin Relaxation

The model of Fig. 16 can also be reconciled with the observation that resonance II disappears above 30 K in the vacuum-fired sample with $x = 0.25$ but remains to above 200 K in sample L (Fig. 7). A proton transfer to a neighboring oxide ion results in a relaxation of the static displacement of the titanium ion towards the opposite oxide ion in the $(TiO)^+$ configuration. Unless the electron transfers to the neighboring site with the proton, the originally trapped electron will undergo rapid spin-relaxation in the titanium-3*d* conduction band resulting in the disappearance of resonance II. In sample L, all of the titanium-3*d* electrons are bound to hydroxyl ions. In the vacuum-fired sample, however, there are a large number of free titanium-3*d* electrons and some of the neighboring titanium ions will be Ti^{3+} ions. In this case, the proton transfer to a neighboring oxide ion does not require a simultaneous electron transfer. This possibility of easy proton transfer lowers the temperature above which a dynamic vibrational mode replaces the static displacement of the titanium ion in the $(TiO)^+$ configuration.

The resonance-I line broadening above 120 K may similarly arise from such a breakdown of the static displacement of the titanium ion. Substitution of lithium ions onto the B sites produces a narrowing of the conduction band. There is no reason to suppose that the donor level would track the edge of this band, and so the energy required to excite an electron from the donor level to the conduction band should increase with x. If a simple thermal ionization is the relaxation mechanism, we would then expect the resonance-I line broadening at a given temperature to decrease rapidly with x. On the other hand, only a gentle decrease with x would be anticipated if the relaxation is caused by a breakdown of the static displacement of the titanium ion as described; a shift of the breakdown to higher temperatures with x would result from a strengthening of the $(TiO)^+$ configuration due to B-site lithium-ion coordination to the oxide ion. Therefore this latter relaxation mechanism seems plausible for resonance I as well as for resonance II.

Appendix

The angular-overlap model is a simple crystal-field model that uses the radial integrals of the wavefunctions as variable parameters (*45*). We present here preliminary results of an angular-overlap-model calculation[2] of the Ti^{3+}-ion g-values for a normal B site in $LiTi_2O_4$ and for a site with an oxygen vacancy in one corner.

In the calculation, the spin-orbit coupling constant was fixed at $\lambda = 154$ cm^{-1}, the value for a free Ti^{3+} ion, and the isotropic orbital-reduction factor was varied over the range $0.5 \leq k \leq 1$. There are two parameters, $E\sigma$ and $E\pi$, that describe the extent of σ and π bonding of the Ti^{3+} ion with the oxide-ion nearest neighbors. In these preliminary calculations, these values were fixed at 7000 and 500 cm^{-1}, respectively. They are related to the cubic-field splitting parameter Δ (Fig. 14) by the relation (*45*)

$$3E\sigma - 4E\pi = \Delta, \qquad (14)$$

and the value of Δ was estimated as 19,000 cm^{-1} from the diffuse-reflectance spectrum of $LiTi_2O_4$ (*11*). The chosen ratio of $E\sigma$ and $E\pi$ is reasonable for octahedrally coordinated titanium in oxides.[2] The resulting g-values for a normal B site are

$$g_x = 1.25,\ g_z = 1.4; \qquad \text{for } k = 0.5$$
$$g_x = 1.0,\ \ g_z = 1.05; \qquad \text{for } k = 1.0. \qquad (15)$$

It is evident that neither resonance I nor

[2] Thanks are due to Dr. M. Gerloch, Dept. of Organic and Inorganic Chemistry, Cambridge University, for the use of his computer program "CAMMAG," together with much helpful advice.

resonance II can originate from an unperturbed site. If one of the oxygen ions is removed, the bonding parameters for the vacancy go to zero. If the bonding parameters for the opposite oxide ion are increased to 10,000 and 800 cm^{-1} to simulate the shift of the Ti^{3+} ion on the apical axis to form a square-pyramidal site, the resulting g-values are

$$g_x = 1.94,\ g_z = 1.92; \qquad \text{for } k = 0.5$$

$$g_x = 2.0,\ g_z = 1.96; \qquad \text{for } k = 1.0. \quad (16)$$

Thus the removal of the oxide ion and shift of the Ti^{3+} ion has increased the calculated g-values toward the free-spin value and produced the required inequality $g_x > g_z$. In fact, with $k = 0.8$ the calculated values are very close to the observed values for resonance I ($g_x = 1.979$, $g_z = 1.951$). Thus the proposed model for resonance I can account qualitatively for the observed g-values.

Acknowledgments

We thank the SERC for financial support and Dr. R. G. Egdell for many fruitful discussions. The magnetic-susceptibility and superconducting-transition-temperature measurements were carried out by MRH at Cornell University under the guidance of Professor M. J. Sienko, and were sponsored by the Air Force Office of Scientific Research under Grant AFOSR 80-0009 and supported in part by the National Science Foundation and the Materials Science Center at Cornell University.

References

1. D. C. JOHNSTON, H. PRAKASH, W. H. ZACHARIASEN, AND R. VISWANATHAN, *Mater. Res. Bull.* **8,** 777 (1973).
2. D. C. JOHNSTON, Ph.D. thesis, University of California—San Diego (1975).
3. D. C. JOHNSTON, *J. Low-Temp. Phys.* **25,** 145 (1976).
4. R. W. MCCALLUM, D. C. JOHNSTON, C. A. LUENGO, AND M. B. MAPLE, *J. Low-Temp. Phys.* **25,** 177 (1976).
5. R. N. SHELTON, D. C. JOHNSTON, AND H. ADRIAN, *Solid State Commun.* **20,** 1077 (1976).
6. S. FONER AND E. J. MCNIFF, *Solid State Commun.* **20,** 995 (1976).
7. U. ROY, A. DAS GUPTA, AND C. C. KOCH, *IEEE Trans. Magn.* **MAG-13,** 836 (1976).
8. A. H. MOUSA AND N. W. GRIMES, *J. Mater. Sci.* **15,** 793 (1980).
9. T. INUKAI, T. MURAKAMI, AND T. INAMURA, *Jap. J. Apl. Phys.* **20,** L264 (1980).
10. T. INUKAI, T. MURAKAMI, AND T. INAMURA, *Jpn. J. Appl. Phys.* **20,** L681 (1981).
11. M. R. HARRISON, D. Phil. thesis, Oxford University (1981).
12. M. R. HARRISON, P. P. EDWARDS, AND J. B. GOODENOUGH, in press.
13. J. B. GOODENOUGH, *Prog. Solid State Chem.* **5,** 145 (1971).
14. N. F. MOTT, "Metal–Insulator Transitions," Taylor & Francis, London (1974).
15. A. DESCHANVRES, B. RAVEAU, AND Z. SEKKAL, *Mater. Res. Bull.* **6,** 699 (1971).
16. J. F. DORRIAN AND R. E. NEWNHAM, *Mater. Res. Bull.* **4,** 179 (1969).
17. U. ROY, K. PETROV, I. TSOLOVSKI, AND P. PESHEV, *Phys. Status Solidi A* **44,** K25 (1977).
18. K. PETROV AND I. TSOLOVSKI, *Phys. Status Solidi A* **58,** K85 (1980).
19. J. C. MIKKELSEN, *J. Amer. Ceram. Soc.* **63,** 331 (1980).
20. G. IZQUIERDO AND A. R. WEST, *Mater. Res. Bull.* **15,** 1655 (1980).
21. B. MOROSIN AND J. C. MIKKELSEN, ACTA CRYSTALLOGR. SECT. B **35,** 798 (1979).
22. L. GASTALDI AND A. LAPICCIRELLA, *J. Solid State Chem.* **30,** 223 (1979).
23. F. J. DYSON, *Phys. Rev.* **98,** 349 (1955).
24. D. J. LOWE, *Biochem. J.* **171,** 649 (1978).
25. J. H. VAN VLECK, *Phys. Rev.* **57,** 426 (1940).
26. R. ORBACH, *Proc. Roy. Soc. London, Ser. A* **264,** 458 (1961).
27. R. KUBO AND Y. TOYAZAWA, *Prog. Theor. Phys.* **13,** 160 (1955).
28. R. D. IYENGAR AND M. CODELL, *Colloid Interface Sci.* **3,** 365 (1972).
29. E. SERWICKA, R. N. SCHINDLER, AND R. SCHUMACHER, *Ber. Bunsenges. Phys. Chem.* **85,** 192 (1981).
30. R. JAMES, Ph.D. thesis, London University (1978).
31. W. D. OHLSEN AND O. W. JOHNSON, *J. Appl. Phys.* **44,** 1927 (1973).
32. L. N. SHEN, O. W. JOHNSON, W. D. OHLSEN, AND J. W. DEFORD, *Phys. Rev. B* **10,** 1823 (1974).
33. R. D. SHANNON, *J. Appl. Phys.* **35,** 3414 (1964).

34. C. R. A. CATLOW AND R. JAMES, Royal Society of Chemistry, Specialist Periodical Report: "Chemical Physics of Solids and Their Surfaces," Vol. 8, p. 108 (1980).
35. A. CARRINGTON AND A. D. MCLACHLAN, "Introduction to Magnetic Resonance," p. 155, Harper, New York (1967).
36. A. ABRAGAM AND B. BLEANEY, "Electron Paramagnetic Resonance of Transition Ions," Oxford Univ. Press (Clarendon), London/New York (1970).
37. K. W. H. STEVENS, *Proc. Roy. Soc. London, Ser. A* **219,** 542 (1953).
38. H. M. GLADNEY AND J. D. SWALEN, *J. Chem. Phys.* **42,** 1999 (1965).
39. L. G. VANQUICKENBORNE, C. GORLLER-WALRAND, AND R. DEBUYST, *J. Chem. Soc. Dalton Trans.* 1150 (1979).
40. J. W. ORTON, "Electron Paramagnetic Resonance," p. 115, Iliffe, London (1968).
41. T. SHIMIZU, *J. Phys. Soc. Jpn.* **23,** 848 (1967).
42. C. N. R. RAO AND K. J. RAO, "Phase Transitions in Solids," p. 310, McGraw–Hill, London (1978).
43. C. J. BALLHAUSEN AND H. B. GRAY, *Inorg. Chem.* **1,** 111 (1962).
44. J. B. GOODENOUGH, *in* "Defects and Transport in Oxides" (M. S. Seltzer and R. I. Jaffee, Eds.), p. 55, Plenum, New York (1973).
45. M. GERLOCH AND R. F. MCMEEKING, *J. Chem. Soc. Dalton Trans.* 2443 (1975).
46. "International Tables for X-Ray Crystallography," Vol. I, Kynoch, Birmingham (1965).